THE RIGA DYNAMO EXPERIMENT ⋆

AGRIS GAILITIS, OLGERTS LIELAUSIS and ERNESTS PLATACIS
Institute of Physics, Latvian University, LV-2169 Salaspils 1, Riga, Latvia
E-mails: gailitis@sal.lv; mbroka@sal.lv; platacis@sal.lv

GUNTER GERBETH and FRANK STEFANI
Forschungszentrum Rossendorf, P.O. Box 510119, D-01314 Dresden, Germany
E-mails: G.Gerbeth@fz-rossendorf.de; F.Stefani@fz-rossendorf.de

(Received 6 December 2001; Accepted 9 January 2003)

Abstract. Cosmic magnetic fields, including the magnetic field of the Earth, are produced by the homogeneous dynamo effect in moving electrically conducting fluids. We sketch the history of the underlying theory and comment on previous attempts to realize homogeneous dynamos in the laboratory. For the main part, we report on two series of experiments carried out at the Riga dynamo facility. In November 1999 a slowly growing magnetic field eigenmode was observed for the first time in a liquid metal experiment. In July 2000, the magnetic field saturation regime was studied and a number of interesting back-reaction effects were observed. A preliminary interpretation of the measured data is also presented.

Keywords: dynamo, magnetic field

1. Background

1.1. TECHNICAL AND NATURAL DYNAMOS

Nowadays, the dynamo effect in homogeneous electrically conducting fluids is widely accepted as the only possible effect to explain the abundance of magnetic fields in the cosmos. All other explanations, starting with Gilbert's interpretation of the Earth as a big lodestone (Gilbert, 1600) and ending with Blackett's hypothesis that large astronomical bodies might have dipole moments that are directly proportional to their angular momentum (Blackett, 1947), had to be discarded over the course of time.

The basic idea of a self-exciting dynamo traces back to von Siemens in 1867 or even to Jedlick in 1861 (see the remarks in Simonyi, 1990). Generally, the possibility for dynamo action arises from the induction of an electromotive force when a conductor moves with the velocity $\mathbf{v}$ in a magnetic field $\mathbf{B}$. The induced current density $\mathbf{j}$ is given by Ohm's law

$$\mathbf{j} = \sigma(\mathbf{E} + \mathbf{v} \times \mathbf{B}), \tag{1}$$

⋆ Based on an invited review, presented at the XXVI General Assembly of the European Geophysical Society, Nice, France, March 2001.

Surveys in Geophysics **24:** 247–267, 2003.

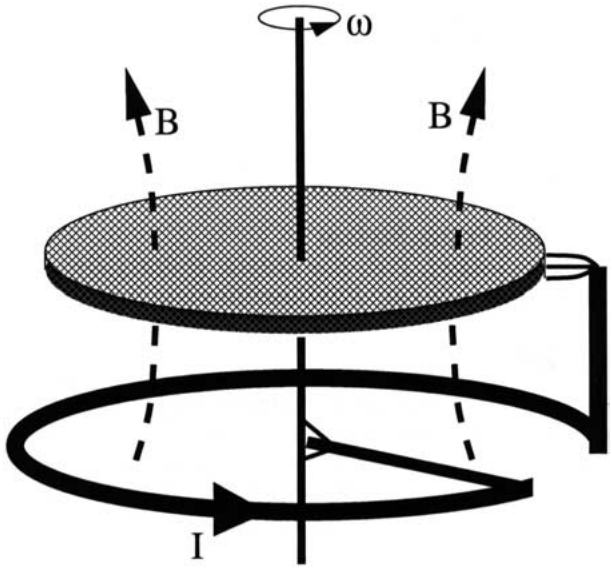

Figure 1. Bullard's disk dynamo. The rotation of the disk in a given magnetic field B induces a current in the wire that amplifies the magnetic field. At a certain critical value of the rotation rate ω, self-excitation occurs.

where σ is the electrical conductivity and $\mathbf{E}$ denotes the electric field.

Leaving aside the specific technical realization, the general question of magnetic field self-excitation is how is it possible for the electric current (Equation (1)) which is generated by the magnetic field also to produce the very same magnetic field. The simplest illustration of such a bootstrap effect is given by the homopolar disk dynamo (Figure 1), basically consisting of a rotating metal disk which is slidingly connected to a wire wound around the rotation axis of the disk (Bullard, 1955). This simple device can work as a self-excited dynamo if the angular velocity ω of the disk exceeds a certain critical value $\omega_c = 2\pi R/L$, with R and L denoting the Ohmic resistance of the circuit and the mutual inductance between the circuit and the rim of the disk, respectively. Although this device looks very simple, one should note the presence of insulating spacings between the conducting parts forcing the current in the desired direction. In contrast to multiply connected and asymmetric technical dynamos of this sort, cosmic dynamos work in singly connected domains with uniform conductivity.

It was after the strong magnetic field in sunspots had been detected by Hale in 1908 that Larmor (1919) suggested self-excitation as the source of magnetic fields of large astronomical bodies, such as the Sun. Later, the dynamo process was adopted as an explanation of the geomagnetic field, too. Early contributions to dynamo theory based on the equations of magnetohydrodynamics (MHD) were made by Elsasser (1946) and Bullard (1949). Since then, much analytical and numerical progress has been made in the understanding of homogeneous dynamos.

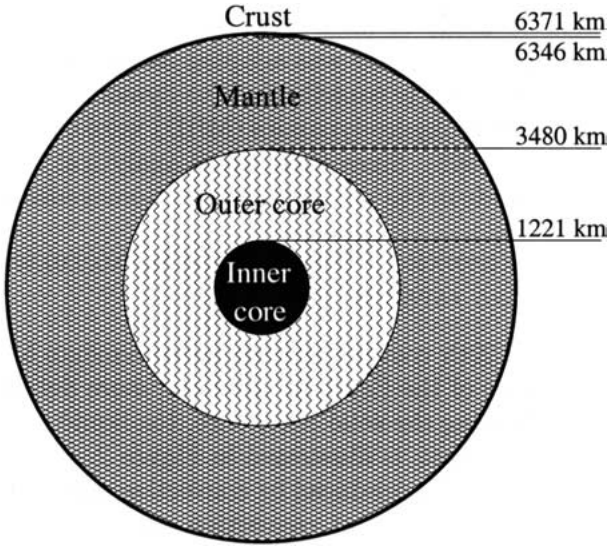

Figure 2. Global structure of the Earth's interior. The magnetic field is produced by convective motion within the liquid outer core.

1.2. THE EARTH'S DYNAMO – OBSERVATIONAL, MATHEMATICAL AND NUMERICAL ASPECTS

In the course of the 20th century, seismic measurements have revealed the internal structure of the Earth in more and more detail. The main shell structure, including the solid inner core, the liquid outer core, the mantle, and the thin crust, is illustrated in Figure 2.

The geomagnetic field is produced by convective motion in the liquid outer core. The main sources of convection are the thermal and/or compositional buoyancy and the Coriolis force. Therefore, thermal and gravitational energy is first transformed into kinetic energy, which in turn is partly transformed into magnetic energy. A comprehensive presentation of geomagnetism can be found in Merrill et al. (1998).

From the mathematical point of view, the occurrence of dynamo action is a bifurcation phenomenon similar to a hydrodynamic instability. Just as a hydrodynamic instability occurs at a certain critical value of the hydrodynamic Reynolds number $Re = Lv/\nu$, where L is a typical length scale of the system, v is a typical velocity scale and ν is the kinematic viscosity, a hydromagnetic instability may occur at a certain critical value of the magnetic Reynolds number $Rm = \mu_0 \sigma L v$, where μ_0 is the permeability of free space and σ is the electrical conductivity of the fluid. The inverse of $\mu_0\sigma$ is called the magnetic diffusivity, often denoted by λ.

Mathematically, this process is described by the so-called induction equation for the magnetic field $\mathbf{B}$,

$$\frac{\partial \mathbf{B}}{\partial t} = \nabla \times (\mathbf{v} \times \mathbf{B}) + \lambda \Delta \mathbf{B} \tag{2}$$

with the constraint

$$\nabla \cdot \mathbf{B} = 0. \tag{3}$$

Without the velocity dependent term on the r.h.s., Equation (2) would simply describe the free decay of a magnetic field in a conducting medium. Given a sufficient twist (or helicity) of the velocity field, at a certain flow intensity it can twist and stretch the magnetic field in such a way that the diffusion may be compensated.

What happens in this case, when the critical magnetic Reynolds number is exceeded? The magnetic field starts to grow exponentially, until the resulting Lorentz forces become large enough to modify the pre-supposed velocity structure. In order to describe this back-reaction it is necessary to solve the Navier–Stokes equation

$$\frac{\partial \mathbf{v}}{\partial t} + (\mathbf{v} \cdot \nabla)\mathbf{v} = -\frac{\nabla p}{\rho} + \frac{1}{\mu_0 \rho}(\nabla \times \mathbf{B}) \times \mathbf{B} + \nu \Delta \mathbf{v} + \mathbf{f}_{\text{drive}}, \tag{4}$$

where the back-reaction of the magnetic field on the velocity is included and the driving forces (in particular the buoyancy force for the geodynamo) are summarily denoted by $\mathbf{f}_{\text{drive}}$. In Equation (4), ρ and ν denote the density and the kinematic viscosity of the fluid, respectively.

The advent of computers has made it possible to simulate the coupled system of Equations (2), (3), and (4) (possibly with an additional equation for the temperature) in detail. The last decade has brought about tremendous progress in the numerical treatment of the geodynamo (Glatzmaier and Roberts, 1995; Kuang and Bloxham, 1997; Busse et al., 1998; Christensen et al., 1999). Most of the recent numerical results share the main features with the Earth's magnetic field, including the dominance of the axial dipolar component, weak non-dipolar structures, and, in some cases, full polarity reversals.

The results of these dynamo simulations could therefore give the impression that the magnetic field generation process of the Earth is completely understood. However, as has been pointed out, e.g., by Busse (2000), the relevance of such numerical simulations for the real Earth core is far from clear. The main obstacle for realistic numerical simulations is the fact that some of the parameters for the Earth are presently not attainable in simulations. This concerns, in particular, the Ekman number E (ratio of rotation time scale to viscous time scale) and the magnetic Prandtl number Pm (ratio of magnetic diffusion timescale to viscous diffusion timescale). The Ekman number of the Earth is of the order 10^{-15}, the magnetic Prandtl number is of the order 10^{-6}. Present numerical simulations are carried out with values of $E \sim 10^{-6}$ and $Pm \sim 0.1$, respectively.

1.3. Past experiments

Until very recently, a notorious problem for the deeper understanding of hydromagnetic dynamos was the lack of any possibility to verify numerical simulations

by experimental results. Taking a glance at realistic numbers of the kinematic viscosity ν and the magnetic diffusivity λ, it immediately becomes clear why a hydromagnetic instability is far from an everyday experience, quite in contrast with hydrodynamic instabilities. While a typical value of ν is 10^{-6} m^2/s (for water at 20 °C), the value of λ for liquid sodium, the best liquid conductor, is 0.1 m^2/s. That means, to get a hydrodynamic instability with a critical *Re* of, say, 100 the product of length and velocity scale has to be $Lv = 10^{-4}$ m^2/s which can easily be achieved, whereas it takes a product of $Lv = 10$ m^2/s for the corresponding hydromagnetic instability to occur. It is this large product which makes laboratory dynamo experiments so expensive. If there were a liquid metal available with a magnetic diffusivity of the order 10^{-6} m^2/s one could produce a nice toy dynamo, with some fixed lamps on it which would light up when the liquid metal inside was shaken in an appropriate manner.

The first laboratory experiment which deserves to be called a homogeneous dynamo, although not a fluid dynamo, was carried out by Lowes and Wilkinson (1963, 1968) in the 1960s. The set-up consisted of two iron cylinders rotating about perpendicular noncrossing axes in a solid block of the same iron. Indeed, self-excitation of a magnetic field was observed when the rotation rate of the cylinders had crossed a critical value. The high value of magnetic permeability ($\mu \sim 150\mu_0$) of the materials used made it possible to reach self-excitation at a reasonably low rotation rate. At the same time the whole phenomenon was controlled by ferromagnetic nonlinearities (remanence of magnetic prehistory, etc.). Needless to say, the most interesting back-reaction effects of the Lorentz forces on the fluid velocity field could not be investigated in such a solid body model.

As one of the first dynamo-problem-related liquid metal experiments, the work of Lehnert (1957) has to be mentioned. In a vessel containing 58 litres of rotating liquid sodium the important poloidal – toroidal magnetic field transformation was demonstrated. By the way, it seems that in Lehnert (1952) the first deduction of the magnetic Reynolds number was presented.

Inspired by the achievements of mean-field magnetohydrodynamics (Steenbeck et al., 1966; Krause and Rädler, 1980), there were considerable activities in the 1960s concerning an experimental observation of the α-effect. In a simple experiment it was demonstrated by Steenbeck et al. (1967) that, in a sodium flow through two helically linked copper ducts, an electric potential difference *parallel* to an applied magnetic field arises which is proportional to the squared sodium velocity. It must be considered as the initial Riga experiment on the subject of the dynamo. In the same year, Gailitis (1967) proposed an experiment with 12 $\times$ 12 spin-generators with the intention to simulate the α^2-dynamo. Later quite a similar model became famous under the synonym Roberts–Busse dynamo as it was the basis for the Karlsruhe dynamo experiment described by Stieglitz and Müller (2001).

For a comprehensive survey of the past and present dynamo experiments and a discussion of their differences we refer the reader to the review paper by Gailitis et al. (2002c). In the following we will focus on the Riga dynamo experiment.

2. As Large as Necessary, as Small as Possible

Concerning the expectations about the necessary dimensions of a laboratory dynamo experiment, it is historically interesting to quote Steenbeck (1975) who wrote "... that remarkable effort would be necessary for such an experiment – a vessel with approximately 10 m^3 of liquid sodium and with a pump rate of not less than 10 m^3/s". In the following we will see how those envisioned dimensions were reduced to 2 m^3 and 0.7 m^3/s, respectively, based on the mathematical consideration of concrete dynamo models.

Only one year later (Gailitis and Freibergs, 1976) the threshold for the convective instability in a helical MHD dynamo (Ponomarenko, 1973) was found. The calculated critical value $Rm = 17.7$ (at the optimum relation of axial to azimuthal velocity components) pointed to considerably lower flow parameters. The value was not changed very much when the model was modified by introducing a counterflow (Gailitis and Freibergs, 1980). However, by means of this counterflow the model was brought closer to experimental reality, the convective instability was transferred into an absolute one, and self-excitation was made possible in a finite length model.

Under the guidance of two of the authors, a forerunner of the present Riga dynamo experiment was carried out in St. Petersburg (Gailitis et al., 1987, 1989). Due to the occurrence of mechanical vibrations, this experiment had to be stopped before magnetic field self-excitation was reached. Nevertheless, it was possible to collect data on the amplification of an external seed field by the dynamo which gave some indication of the value of the critical magnetic Reynolds number which was in surprisingly good agreement with theoretical predictions from the above models.

2.1. Fine-tuning a huge machine

The Riga dynamo experiment is the technical realization of what could be called an "elementary cell" of all hydromagnetic dynamos: a screw motion. The main idea traces back to the paper of Ponomarenko (1973) who considered magnetic field self-excitation caused by the screw motion of an electrically conducting solid body within a medium, at rest, with the same conductivity.

As mentioned, an important modification of the original Ponomarenko model which turns the convective instability of this model into an absolute instability is the addition of a coaxial back-flow. In principle, this arrangement would be sufficient to build a dynamo. However, it is useful to add a third co-axial cylinder containing

sodium at rest. This part makes electric currents close in a larger volume which results in a decrease of the Ohmic losses.

The magnetic field that can self-excite in such a flow configuration rotates about the vertical symmetry axis in the same direction as the rotational component of the flow, but much slower. This rotation produces, at a fixed position, an alternating magnetic field. Note that this field rotation in the considered case follows from the linear, kinematic dynamo theory. Hence, it has more in common with the solar magnetic cycle than with the chaotic field reversals of the Earth which are believed to be due to non-linear effects.

Making a reasonable assumption about the relative costs for the construction and operation of the experiment, Gailitis (1989, 1996) optimized the main geometric relations of the facility, i.e., the pitch of the screw motion and the relation of the diameters of the three cylinders to each other as well as to the length of the system. The whole facility is sketched in Figure 3.

Based on this preliminary optimization, a water dummy facility with basically the same size and geometry as the later sodium facility was installed in order to carry out hydraulic pre-experiments. A very important point was to ensure the mechanical integrity of the system under the strong mechanical strains which are inevitable for this kind of experiment. A lot of effort has been put into vibrational measurements using this water facility and into numerical simulations of the interaction between the fluid and the walls in order to prevent any dangerous situation from occurring (Altstadt, 1997).

2.2. TAILORING VELOCITY PROFILES

After having fixed the main geometry of the facility it was necessary to optimize the velocity profiles in order to ensure that self-excitation occurs within the limited power resources. As in an air test after the 1987 experiment (Gailitis, 1992), the first velocity measurements in the water dummy facility had revealed velocity profiles quite different from the solid body rotation profile which was supposed in most underlying numerical investigations of Ponomarenko-like dynamos. The azimuthal velocity was concentrated near the axis, and decreasing outwards. While the critical Rm for the solid body rotation profile was calculated to be approximately 18 (for the absolute instability) the corresponding number for the measured profiles turned out to be 31. However, the available power resources of about 120 kW allowed only a maximum Rm of approximately 23 to be reached. In a long iterative process involving theoretical and numerical profile optimization (Stefani et al., 1999), pump design and velocity measurements using the water dummy facility (Christen et al., 1998), it was possible to tailor velocity profiles which we considered to be suitable for magnetic field self-excitation. To achieve this goal, vane arrays were inserted in front of, and behind, the propeller. The last velocity measurements at the Riga water dummy facility had revealed, for a rotation rate of 2000 rpm, an

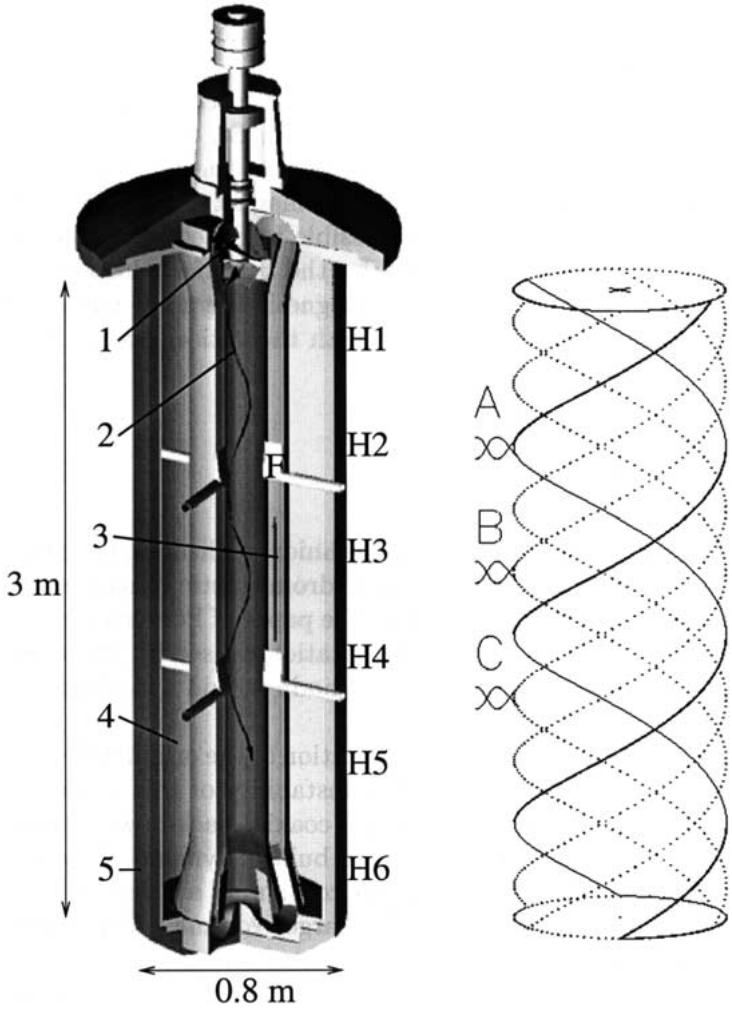

Figure 3. The central module of the Riga dynamo facility. Main parts are: 1, Propeller; 2, Helical flow region; 3, Back-flow region; 4, Sodium at rest; 5, Thermal insulation; F, Position of the fluxgate sensor; H1 . . . H6, Positions of the Hall sensors. The right hand side shows the seed field coil which must be imagined to be wound around the central module. This coil was mainly used in the subcritical regime to study the amplification of an applied magnetic field. The direction of rotation of the field around the vertical axis can be adjusted by two different settings of the 3-phase current in the coils A, B, and C.

axial velocity of about 15 m/s at the centre of the inner cylinder and an azimuthal velocity of about 9 m/s close to the innermost wall.

In connection with these preparations, a 1 : 2 water model of the hydraulic part of the dynamo was build at the Technical University of Dresden. Using Laser-Doppler-Velocimetry, this model allowed the mean velocity fields and the turbulent fluctuations to be studied in more detail than in water tests of the real facility.

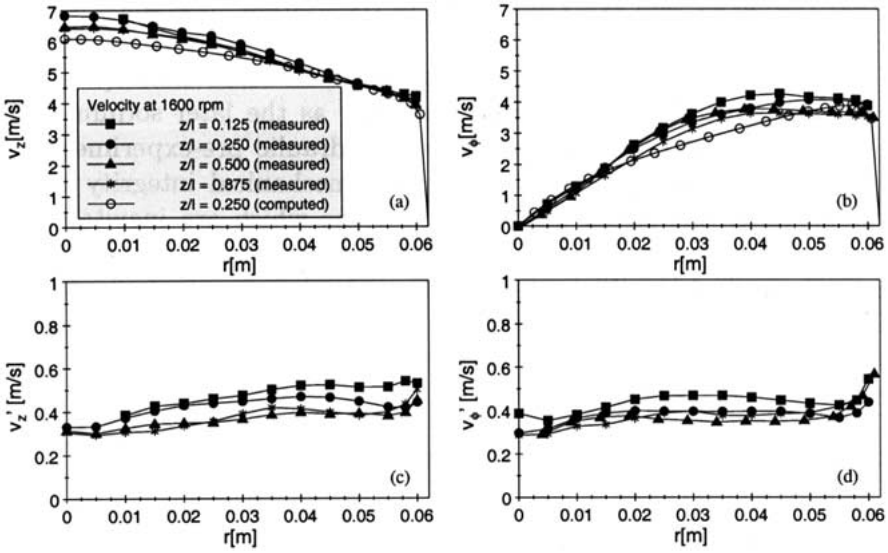

Figure 4. Velocity profiles measured with a 1 : 2 water test model at the Dresden University of Technology (Christen, 2000). Apart from an overall scaling factor of approximately 2, the flow profiles can be considered as equivalent to the real flow at the Riga sodium facility. Measured mean axial (a) and azimuthal (b) components at different distances from the propeller, and the corresponding fluctuations $v' = \sqrt{\langle(\Delta v)^2\rangle}$(c) and (d).

Figure 4 shows the axial (a) and the azimuthal (b) velocity profiles and the corresponding fluctuations (c, d) measured in the central tube of this 1:2 water model. The velocity profiles differ significantly from the solid body rotation profiles. Nevertheless, in numerical simulations such profiles give dynamo action more easily than for solid body profiles with the same flowrate and angular momentum. Apart from an overall scaling factor, these profiles can be considered as reasonable approximations of the flow in the real sodium facility. As turbulence is less than 10 per cent of the mean flow, its influence on the generation conditions was estimated to be negligible.

3. From Self-Excitation to Saturation

It is quite usual in dynamo theory to divide the models considered into kinematic models and dynamically consistent (or MHD) models. In the former, the fluid velocity is considered as given. In the latter, the magnetic field, after having grown exponentially in an initial phase, acts back on the flow by virtue of the Lorentz forces. The dynamo experiments carried out at the Riga sodium facility followed exactly this scheme. In the first experiment in November 1999 a positive growth rate of the magnetic field was reached, but only barely (Gailitis et al., 2000). The study of the back-reaction took place in a second series of experiments in July

2000 (Gailitis et al., 2001a). More details of the experiments have been published (Gailitis et al., 2001b, c, d, 2002a, b).

3.1. NOVEMBER 1999

A first series of experiments was carried out from 6–11 November 1999. After having filled the whole dynamo module, sodium was pumped slowly through the channels at 300 °C for 24 hours in order to ensure good electrical contact between the walls and the sodium. For the understanding of the following it is useful to outline the original schedule for this experiment. The main experiment was planned at a temperature of about 150 °C. During cooling down from 300 °C to 150 °C, two pre-experiments were planned at 250 °C and 200 °C. At 250 °C, self-excitation was not expected to occur. At 200 °C this question was open. Unfortunately, after the last run at about 210 °C the experiment had to be stopped due to some technical problems with a seal.

The main purpose of these pre-experiments was to test the response of the dynamo to an externally applied magnetic field which was produced by seed field coils fed by a 3-phase current of any desired low frequency. This seed field coil, which is shown on the r.h.s. of Figure 3, produces a three-dimensional, rotating magnetic field quite similar to the expected eigenfield of the dynamo.

Figure 5 shows the inverse relation of the measured magnetic field to the applied current in the seed field coils for a feeding frequency of 1 Hz versus the rotation rate of the propeller. The squares and crosses correspond to two different settings of the 3-phase current in the seed field coils A, B, and C (cf. Figure 3) with respect to the propeller rotation. An increasing amplification of the seed field can clearly be identified until a rotation rate of 1800 rpm. Above this value, the amplification decreases slightly which has to do with passing by the eigenfrequency, i.e., the rotation rate of the magnetic field eigenmode, of the dynamo. Note that all points in Figure 5, except the rightmost cross, correspond to very clean sinusoidal signals of the same 1 Hz frequency as the seed field. In this regime, there is strong amplification *without self-excitation*. When switching off the current in the seed field coils, the magnetic field decays.

Figure 6 shows, for a period of 3 seconds, such a field decay as recorded by the six Hall sensors H1–H6 (cf. Figure 3) at a rotation rate of 1980 rpm. From the curves one can infer a decay rate of $p = -0.3\ \mathrm{s}^{-1}$ and a frequency of $f = 1.1$ Hz. The observed amplitude and phase relations at the different sensors were in good correspondence with the predicted magnetic field structure.

After having identified a decaying mode by its well defined features decay rate, frequency, and phase relation, we now come back to the rightmost cross in Figure 5. At this rotation rate (2150 rpm), the fluxgate sensor recorded a new sort of signal which is shown in Figure 7. This signal can be decomposed, with a high statistical significance (Gailitis et al., 2000), into the usual amplified 1 Hz signal

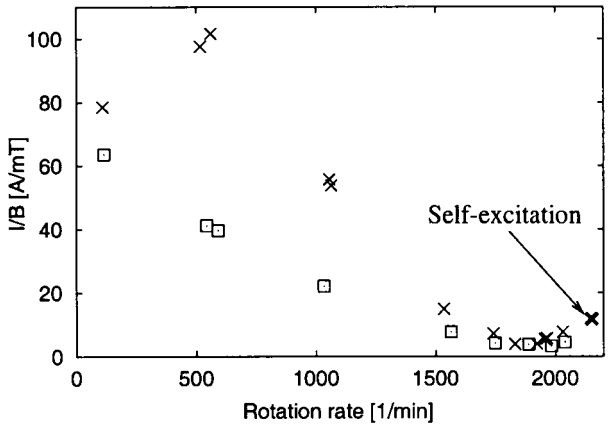

Figure 5. Magnetic field amplification depending on the propeller rotation rate for a seed field frequency $f = 1$ Hz. The ordinate axis shows the inverse relation of the measured magnetic field to the current in the seed field coils. Squares and crosses correspond to two different settings of the 3-phase current in the seed field coils with respect to the propeller rotation. At the highest rotation rate of 2150 rpm, self-excitation occurred, in addition to the amplification of the seed field.

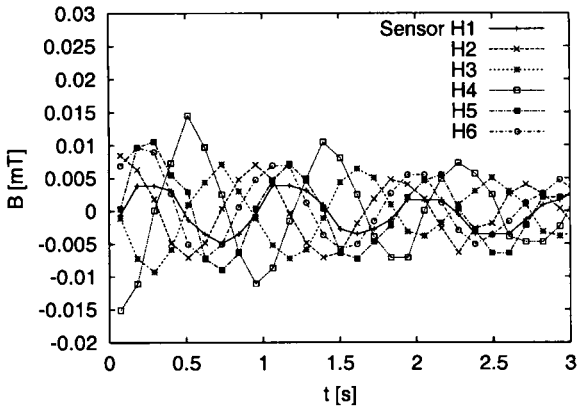

Figure 6. Magnetic fields measured at the Hall sensors H1 ... H6 (see Figure 3) outside the dynamo module, after switching off the coil current. The rotation rate was 1980 rpm. The amplitude and phase relations between the different points are in good correspondence with the predictions from kinematic dynamo theory.

and another signal with a frequency of $f = 1.326$ Hz and a *positive* growth rate of $p = +0.03\ \mathrm{s}^{-1}$.

Our interpretation of the signal shown in Figure 7 is that it is a superposition of two *independent* magnetic field modes which are clearly identifiable by their frequencies. Of course, in order to explain the initial amplitude of the 1.3 Hz mode one has to consider that during the last acceleration phase (before the rotation rate had reached the maximum of 2150 rpm) a mixture of frequencies was born out of the 1 Hz mode due to the time dependence of the velocity. After this acceler-

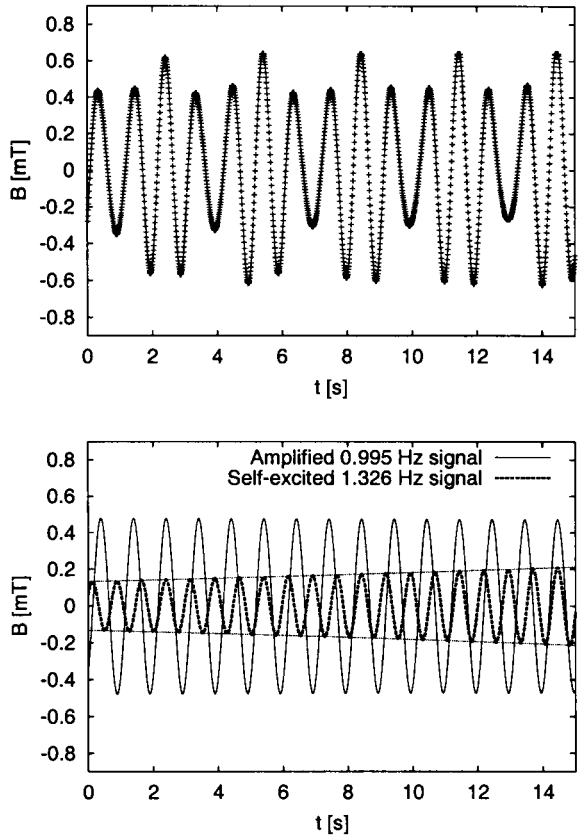

Figure 7. Magnetic field signal recorded by the fluxgate sensor at the highest rotation rate of 2150 rpm (above). Decomposition of the signal into two modes with different frequencies (below).

ation phase, however, the mixture of modes evolved in agreement with kinematic dynamo theory: the 1 Hz mode continued to be amplified, and all modes with different frequencies showed the usual exponential time dependence. All but one modes were decaying. Only the mode with the eigenfrequency of the dynamo at the rotation rate reached survived and continued to grow exponentially.

At this point we mention that the two growth rates and the two frequencies measured in the November experiment fit smoothly into the data which were measured in the July experiment (Figure 10). This correspondence gives strong support for our interpretation.

3.2. JULY 2000

In July 2000 it was possible to work at considerably lower sodium temperatures (around 160 °C), hence at higher Rm (due to the temperature dependence of the electrical conductivity). Figure 8 gives an overview of the four experimental runs which were carried out from 22–25 July 2000. Shown are the rotation rate as well as

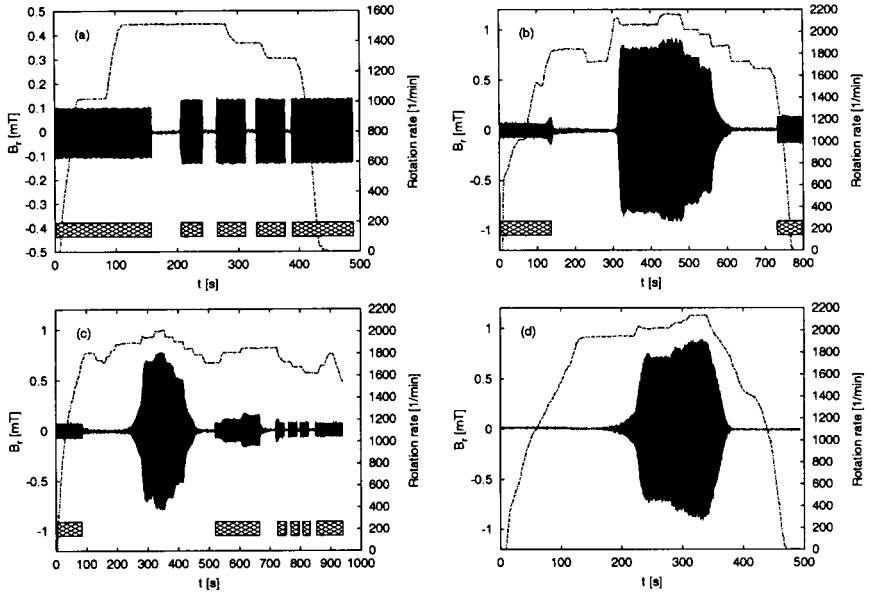

Figure 8. Four experimental runs in July 2000. Rotation rate of the motors, and oscillatory part (any DC-part has been filtered out) of the magnetic field measured at Hall sensor H4 (cf. Figure 3). The periods with external excitation are marked with rectangular bars. First test run at 210 °C without self-excitation; the recorded field is the amplified field of the seed field coils (a). In (b) and (c) there are periods with and without a seed field. The larger amplitude signals are recorded during self-excitation. In (d) the seed field coils were switched off during the whole run. Note the different ordinate scales between (a) and (b)–(d).

the oscillatory part of the magnetic field signal recorded at the selected Hall sensor H4 (cf. Figure 3). Figure 8a illustrates the first run at a temperature of about 210 °C. Intended mainly as a test, this run was carried out completely in the subcritical regime; the signal shown is therefore always the amplified 1 Hz signal of the seed field coils. The next three runs were carried out at temperatures around 160 °C. Figures 8b and 8c contain periods with and without the seed field. Perhaps the clearest run is documented in Figure 8d where no seed field was used at all. Here it is shown how the signal "emerges from nothing" after the rotation rate has reached a critical value (approximately 1920 rpm) and how the field amplitude saturates at levels dependent on the rotation rate.

Some more details from the start and the end of this run are depicted in Figure 9. The first interesting detail here is how the Earth's magnetic field is "pushed out" of the dynamo when the rotation rate runs from 500 to 1000 rpm (a) and how it is "let in" again when the rotation rate is decreased at the end of the run (d). This behaviour is nothing other than the usual skin effect. The vertical component of the ambient magnetic field is seen to be a bit less than 0.1 mT which is higher than one would expect from geomagnetic data. Note, however, that the dynamo facility is inside a steel-concrete building and that it is mounted on a frame made of custom

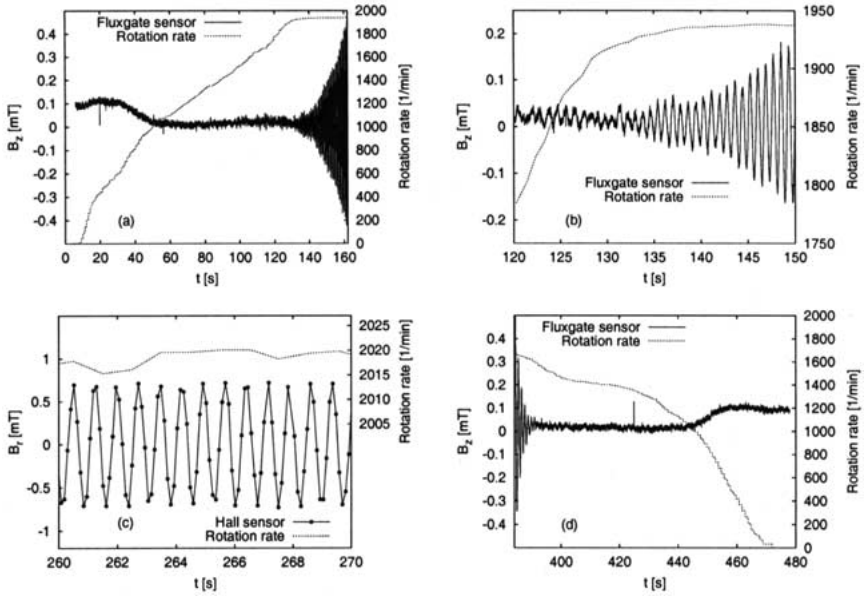

Figure 9. Details of the magnetic field measurement for the run shown in Figure 8(d). The pushing out (a) and "letting in again" (d) of the Earth's magnetic field, and the beginning of the self-excitation (b), and details in the saturation regime (c) on an expanded scale, are evident. Data for (a), (b), (d) are from the flux-gate sensor, data for (c) are from the Hall sensor H4 (cf. Figure 3). Note that the convention for the direction of the z-axis used here is reversed to the direction in the remaining text.

steel (the very dynamo module is, of course, made from austenitic, non-magnetic steel).

The most interesting details are the self-excitation of a rotating magnetic field which starts at $t = 130$ s (b) and the magnetic field evolution within the saturation regime (c).

From the experimental runs documented in Figure 8, many data concerning growth rates, frequencies, phase relation, and saturation levels were collected.

4. Experimental Data and Their Interpretation

In the following we compile the most important experimental data of the November and July experiments, and present a preliminary interpretation of them.

4.1. Experimental data

Let us start with the dependence of the growth rates and frequencies on the rotation rate. Figure 10 shows the measured data together with the numerical predictions. In order to assess the quality of these predictions they should be described in more detail. Basically, the predictions are the outcome of 2D calculations using a time-

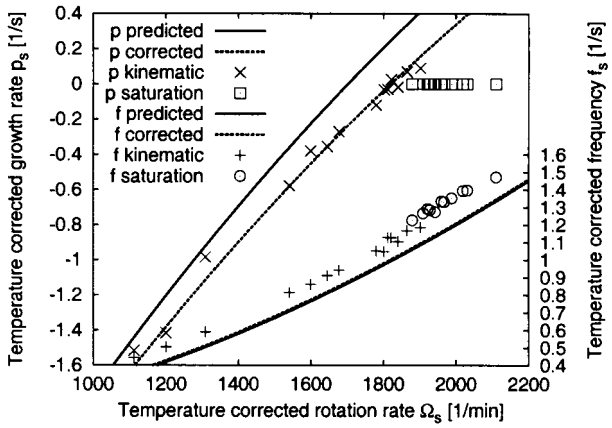

Figure 10. Measured growth rates p and frequencies f for different rotation rates in the kinematic and the saturation regime, compared with the numerical predictions. Note that the measurements presented are made at different temperatures T, hence at different electrical conductivities $\sigma(T)$ of sodium. To have a common reference temperature we use the scaling rules of the induction equation and scale the rotation rate Ω as well as the growth rate p and the frequency f to $(\Omega_s, p_s, f_s) = \sigma(T)/\sigma(157\,^\circ\mathrm{C})(\Omega(T), p(T)f(T))$. The full lines show the numerical predictions for p_s and f_s made with a 2D code which, however, does not take into account the less conducting stainless steel walls. The dashed lines show the predictions which are corrected by 1D simulations incorporating the effect of the walls.

dependent finite-difference solver for the induction Equation (2) in a finite cylinder geometry (Stefani et al., 1999). Note that the effect of the finite thickness of the (non-magnetic) stainless steel inner walls was not included in this code. However, it was known from 1D calculations (Gailitis, 1996) that the overall effect of the walls amounts to an increase of about 8 per cent for the critical magnetic Reynolds number. The corresponding correction, as it results from 1D calculations, is implemented in the curves "p corrected" and "f corrected". Remarkably, the measured growth rates are met perfectly by this correction, whereas the very small frequency correction cannot explain the deviation from the measured frequencies.

Concerning the input data base for these computations, it should be mentioned that the velocity inside the dynamo module was not very accurately known. In the water dummy channel the velocity was measured at six different heights along the z-axis and was therefore quite well known. When the final stainless steel construction for the sodium experiment was tested with water the velocity was measurable at only two positions (approximately at 1/3 and at 2/3 of the total tube length). With sodium no velocities have been measured up to the present. Therefore, the velocity inside the tube is not very precisely known.

In view of all these uncertainties, the correspondence of the measured data with the predictions in Figure 10 is quite surprising. The corrected prediction curve for the growth rate fits very well to the measured values. Concerning the corrected prediction for the frequency, there is an overall shift of the measured values of less than

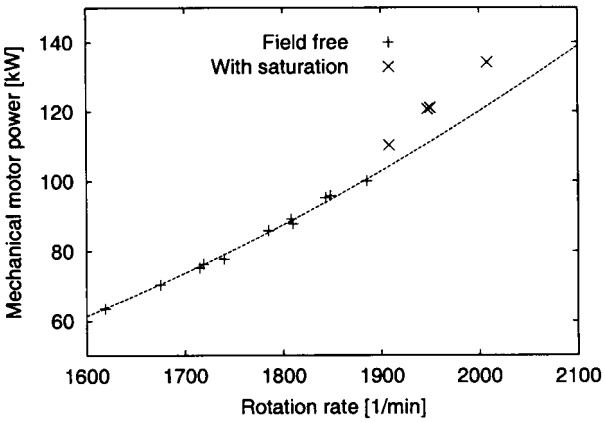

Figure 11. Measured motor power in the kinematic regime and the saturation regime as a function of the rotation rate Ω. The dashed line represents an Ω^3-fit to the data in the field-free regime. In the saturation regime, an excess power of the order of 10 kW is visible.

10 per cent towards lower rotation rates. For both growth rates and frequencies, the slopes of the curves are in good agreement with the predictions.

Most of the data in the kinematic regime were recorded when the excitation was switched off and the decay of the magnetic field was observed. The few points with positive growth rate correspond to the starting phase of self-excitation when the saturation regime had not yet been reached. In Figure 10, there are also some data points which were taken within the saturation regime. It is interesting to observe that the frequency in the saturation regime is not very different from what would be expected from simply extrapolating the kinematic regime, whereas the growth rate in the saturation regime is naturally zero. This is a surprising fact which indicates that there must be a significant deformation of the fluid velocity apart from an overall pressure increase due to the axial Lorentz force.

As for this pressure increase, we have measured the motor power which is needed to maintain a certain rotation rate. Figure 11 shows the power for the field-free and for the saturation regime as a function of the rotation rate Ω. In the field-free regime we find the usual Ω^3-dependence which is well-known in hydraulics. In the saturation regime the power consumption is greater than the Ω^3-fit by approximately 10 kW. This is the excess power which the motor has to provide in order to overcome the additional pressure due to the Lorentz forces.

Let us consider now Figure 12 where, for three of the Hall sensors, the dependence of the magnetic field saturation amplitude on the rotation rate is given. Evidently, this dependence is not homogeneous along the z-axis. For a higher rotation rate, there is a remarkable shift of the field maximum towards the pump region.

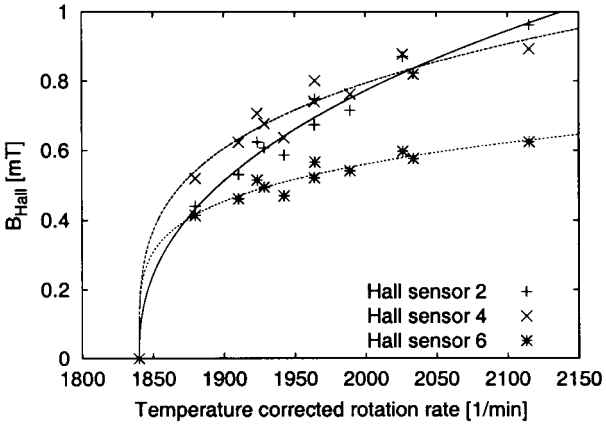

Figure 12. Measured magnetic field levels at the Hall sensors H2, H4, H6 (see Figure 3) in the saturation regime. The lines are fit curves of the form $\sim (\Omega_c - 1940\ \mathrm{min}^{-1})^{\beta}$ with $\beta = 0.417$ for H2, $\beta = 0.275$ for H4, $\beta = 0.216$ for H6. The temperature corrected rotation rate Ω is related to the measured rotation rate Ω via $\Omega_c(T) = \sigma(T)/\sigma(157\,^{\circ}\mathrm{C})\Omega$.

4.2. A SIMPLE MODEL OF BACK-REACTION

Even without having carried out a fully non-linear simulation of the saturation regime, we can attempt to understand the essential features of the back-reaction. Consider, for the sake of simplicity, only the Lorentz force terms without angular dependence (there are also terms proportional to $\exp(2i\phi)$ resulting from the excited magnetic field which is proportional to $\exp(i\phi)$. It is conceivable that the axial and the radial components of this force are, to a large extent, absorbed into pressure resulting in a motor power increase. The angular component of this force, however, cannot be absorbed into pressure and is therefore constrained to brake the angular velocity component.

One may now ask if such an accumulating braking of the azimuthal velocity component could be responsible for the two non-trivial saturation effects, namely, the fact that the frequency (quite in contrast to the growth rate) seems to be generally unaffected by the back-reaction, and the field maximum shift towards the pump.

For this purpose we consider a simplified model of back-reaction, including only the azimuthal component of the Lorentz force and its influence on the azimuthal velocity component. We start our simulation with a partly measured, partly interpolated velocity field. The azimuthal component $\bar{v}_\phi$ of this unperturbed velocity is depicted in Figure 13a (for all the following plots we concentrate on the central parts of the inner tube and the back-flow tube). We use the kinematic 2D solver in order to compute the magnetic field structure and the Lorentz forces resulting for this unperturbed flow. The magnetic field strength is fixed in such a way that the power increase due to the action of the Lorentz forces reaches the measured value of 10 kW. Using a linearized and non-viscous version of Equation (4), the

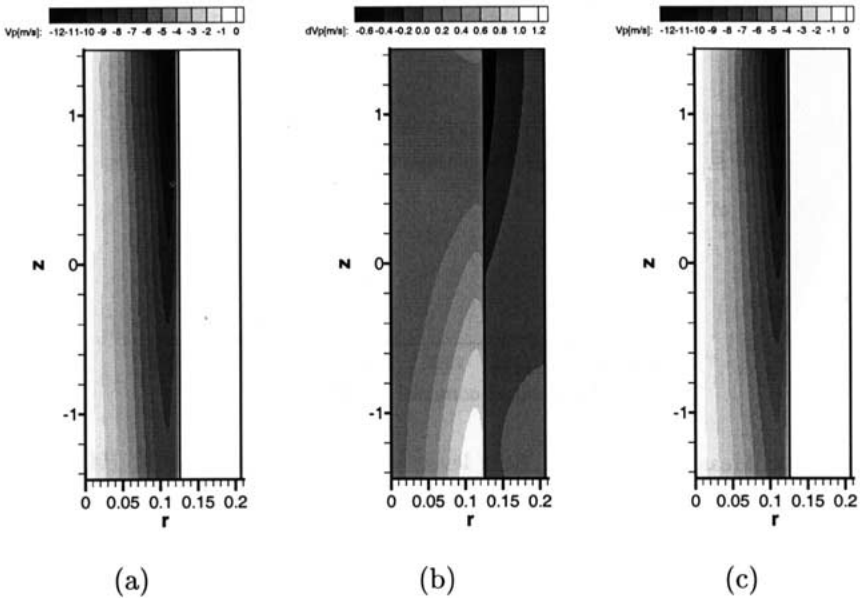

Figure 13. Effect of the Lorentz forces on the azimuthal velocity within the central parts of the innermost cylinder and the back-flow cylinder. Original azimuthal velocity $\bar{v}_\phi$ (a), velocity perturbation δv_ϕ (b), and total velocity $v_\phi = \bar{v}_\phi + \delta v_\phi$ (c).

azimuthal component of the Lorentz force is then used to compute the perturbation δv_ϕ (Figure 13b) and the total azimuthal velocity component $v_\phi = \bar{v}_\phi + \delta v_\phi$ (Figure 13c).

We see that the braking effect is accumulating downward, reaching approximately 1.2 m/s at the bottom, which is 10 per cent of the unperturbed flow. In the back-flow tube, the accelerating effect is accumulating upward, reaching approximately 0.6 m/s at the top.

The resulting perturbed velocity v_ϕ can now be put again into the induction equation solver in order to see the effect on the magnetic field structure and the eigenvalue. It turns out that the perturbed velocity indeed leads to the measured shift of the eigenvalue *and* to the observed upward move of the magnetic field structure. The latter is illustrated in Figure 14, where the measured and the numerically computed magnetic field amplitudes are shown for both the kinematic and the saturation regime.

Of course, these considerations have to be supported by more sophisticated back-reaction simulations. Nevertheless, our back-reaction model gives the first reasonable estimate for the basic mechanism of magnetic field saturation in the Riga dynamo experiment.

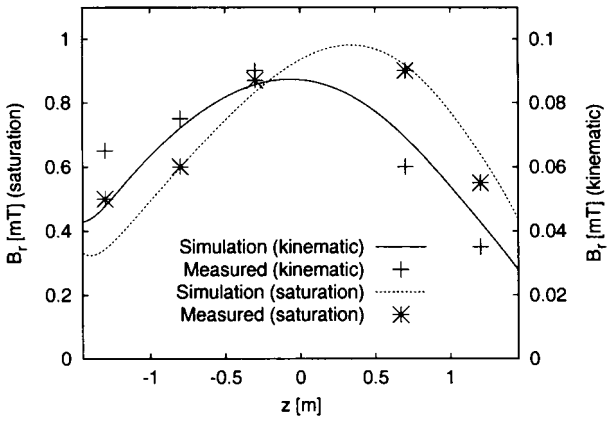

Figure 14. Measured and simulated magnetic field profiles at the Hall sensors. The values in the kinematic regime were taken at a rotation rate of 1945 rpm at the time 210 sec (the very beginning in Figure 8d). The values in the saturation regime are for a rotation rate of 2100 rpm.

5. Conclusions and Prospects

The complementary experiments in Riga and Karlsruhe (Stieglitz and Müller, 2001) have just opened the door into the experimental branch of dynamo science. While in the Riga facility a magnetic field is produced that rotates and varies spatially on the same scale as the generating flow, the field in the Karlsruhe facility is basically a constant one whose large scale part is fed by the small scale flows in the 52 spin generators used.

With respect to the large effort which was necessary to make these experiments run, the expense in carrying out additional experimental runs will be relatively low. Evidently, the Riga experiments have shown already interesting and non-trivial back-reaction effects. Although the power resources are not very large it will be interesting to study these effects in great detail in order to understand this paradigmatic case of magnetic field saturation. In order to do that, much numerical work will be necessary. In addition, measurement of the velocity changes due to the back-reaction would be very desirable.

Acknowledgements

We thank the Latvian Science Council for support under grants 96.0276 and 01.0502, the Latvian Government and the International Science Foundation for support under joint grant LJD100, the International Science Foundation for support under grant LFD000 and the Deutsche Forschungsgemeinschaft for support under INK 18/A1-1. We are grateful to W. Häfele for his interest and support, and to the whole experimental team for preparing and running the experiment.

References

Altstadt, E.: 1997, Internal report, FZ Rossendorf, Dresden.

Blackett, P. M. S.: 1947, 'The Magnetic Field of Massive Rotating Bodies', *Nature* **159**, 658–666.

Bullard, E. C.: 1949, 'The Magnetic Field within the Earth', *Proc. Roy. Soc. London* **A197**, 433–453.

Bullard, E. C.: 1955: 'The Stability of a Homopolar Disc Dynamo', *Proc. Camb. Phil. Soc.* **51**, 744–760.

Busse, F. H.: 2000, 'Homogeneous Dynamos in Planetary Cores and in the Laboratory', *Annu. Rev. Fluid Mech.* **31**, 383–408.

Busse, F. H., Grote, E., and Tilgner, A.: 1998, 'On Convection Driven Dynamos in Rotating Spherical Shells', *Stud. Geophys. Geod.* **42**, 1–6.

Christen, M.: 2000, personal communication.

Christen, M., Hänel, H., and Will, G.: 1998, 'Entwicklung der Pumpe für den hydrodynamischen Kreislauf des Rigaer "Zylinderexperimentes" ', in W. H. Faragallah and G. Grabow (eds.), *Beiträge zu Fluidenergiemaschienen 4*, Faragallah-Verlag und Bildarchiv, Sulzbach/Ts., pp. 111–119.

Christensen, U., Olson, P., and Glatzmaier, G. A.: 1999, 'Numerical Modeling of the Geodynamo: A Systematic Parameter Study', *Geophys. J. Int.* **138**, 393–409.

Elsasser, W. M.: 1946: 'Induction Effects in Terrestrial Magnetism. 1. Theory', *Phys. Rev.* **69**, 106–116.

Gailitis, A.: 1967, 'Self-Excitation Condition for a Laboratory Model of a Geomagnetic Dynamo', *Magnetohydrodynamics* **3**(3), 23–29.

Gailitis, A.: 1989, 'The Helical MHD Dynamo', in H. K. Moffatt and A. Tsinober (eds.), *Topological Fluid Mechanics*, Proc. IUTAM Symposium, Cambridge, U.K., August 13–18, 1989, Cambridge University Press, Cambridge, pp. 147–156.

Gailitis, A.: 1992, 'Experimental Aspects of a Laboratory Scale Liquid Sodium Dynamo Model', in M. R. E. Proctor, P. C. Matthews, and A. M. Rucklidge (eds.), *Theory of Solar and Planetary Dynamos*, Proceedings of NATO ASI, 20.9–2.10, 1992, Cambridge University Press, Cambridge, pp. 91–98.

Gailitis, A.: 1996, 'Project of a Liquid Sodium MHD Dynamo Experiment', *Magnetohydrodynamics* **32**, 58–62.

Gailitis, A. and Freibergs, Ya.: 1976, 'Theory of a Helical MHD Dynamo', *Magnetohydrodynamics* **12**, 127–129.

Gailitis, A. and Freibergs, Ya.: 1980, 'Nature of the Instability of a Turbulent Dynamo', *Magnetohydrodynamics* **16**, 116–121.

Gailitis, A., Karasev, B. G., Kirillov, I. R., Lielausis, O. A., Luzhanskii, S. M., Ogorodnikov, A. P., and Preslitskii, G. V.: 1987, 'Liquid Metal MHD Dynamo Model Experiment', *Magnetohydrodynamics* **23**, 349–353.

Gailitis, A., Karasev, B. G., Kirillov, I. R., Lielausis, O. A., and Ogorodnikov, A. P.: 1989, 'The Helical MHD Dynamo', in J. Lielpeteris and R. Moreau (eds.), *Liquid Metal Magnetohydrodynamics*, Kluwer, Dordrecht, pp. 413–419.

Gailitis, A., Lielausis, O., Dement'ev, S., Platacis, E., Cifersons, A., Gerbeth, G., Gundrum, Th., Stefani, F., Christen, M., Hänel, H., and Will, G.: 2000, 'Detection of a Flow Induced Magnetic Field Eigenmode in the Riga Dynamo Facility', *Phys. Rev. Lett.* **84**, 4365–4368.

Gailitis, A., Lielausis, O., Platacis, E., Dement'ev, S., Cifersons, A., Gerbeth, G., Gundrum, Th., Stefani, F., Christen, M., and Will, G.: 2001a, 'Magnetic Field Saturation in the Riga Dynamo Experiment', *Phys. Rev. Lett.* **86**, 3024–3027.

Gailitis, A., Lielausis, O., Platacis, E., Gerbeth, G., and Stefani, F.: 2001b, 'On the Results of the Riga Dynamo Experiments', *Magnetohydrodynamics* **37**(1/2), 71–79.

Gailitis, A., Lielausis, O., Platacis, E., Gerbeth, G., Stefani, F.: 2001c, 'Riga Dynamo Experiment', in P. Chossat, D. Armbruster, and I. Oprea (eds.), *Dynamo and Dynamics, a Mathematical Chal-*

lenge, NATO Science Series II: Mathematics, Physics and Chemistry, Vol. 26, Kluwer, Dordrecht, pp. 9–16.

Gailitis, A., Lielausis, O., Platacis, E., Gerbeth, G., and Stefani, F.: 2001d, 'Stirring up a Magnetic Field in the Riga Dynamo Experiment', *Proceedings of the XV-me Congres Francais de Mecanique, Nancy 3–7 Septembre, 2001*, CD, article 694, p. 6.

Gailitis, A., Lielausis, O., Platacis, E., Dement'ev, S., Cifersons, A., Gerbeth, G., Gundrum, Th., Stefani, F., Christen, M., and Will, G.: 2002a, 'Dynamo Experiments at the Riga Sodium Facility', *Magnetohydrodynamics* **38**(1/2), 5–14.

Gailitis, A., Lielausis, O., Platacis, E., Gerbeth, G., and Stefani, F.: 2002b, 'On Back-Reaction Effects in the Riga Dynamo Experiment', *Magnetohydrodynamics* **38**(1/2), 15–26.

Gailitis, A., Lielausis, O., Platacis, E., Gerbeth, G., and Stefani, F.: 2002c, 'Laboratory Experiments on Hydromagnetic Dynamos', *Rev. Mod. Phys.* **74**, 973–990.

Gilbert, W.: 1600, *De Magnete*, translated by P. F. Mottelay, Dover, New York, 1958.

Glatzmaier, G. A. and Roberts, P. H.: 1995, 'A Three-Dimensional Self-Consistent Simulation of a Geomagnetic Field Reversal', *Nature* **377**, 203–209.

Krause, F. and Rädler, K.-H.: 1980, *Mean-Field Magnetohydrodynamics and Dynamo Theory*, Akademie-Verlag, Berlin.

Kuang, W. and Bloxham, J.: 1997, 'An Earth-Like Numerical Dynamo Model', *Nature* **389**, 371–374.

Larmor, J.: 1919, 'How Could a Rotating Body Such as the Sun Become a Magnet?', *Rep. Brit. Assoc. Adv. Sci.* 1919, 159–160.

Lehnert, B.: 1952, 'On the Behaviour of an Electrically Conducting Liquid in a Magnetic Field', *Arkiv för Fysik* **5**(5), 69–90.

Lehnert, B.: 1957, 'An Experiment on Axisymmetric Flow of Liquid Sodium in a Magnetic Field', *Arkiv för Fysik* **13**(10), 109–116.

Lowes, F. J. and Wilkinson, I.: 1963, 'Geomagnetic Dynamo: A Laboratory Model', *Nature* **198**, 1158–1160.

Lowes, F. J. and Wilkinson, I.: 1968, 'Geomagnetic Dynamo: An Improved Laboratory Model', *Nature* **219**, 717–718.

Merrill, R. T., McElhinny, M. W., and McFadden, P. L.: 1998, *The Magnetic Field of the Earth: Paleomagnetism, the Core, and the Deep Mantle*, Academic Press, San Diago.

Ponomarenko, Yu. B.: 1973, 'On the Theory of Hydromagnetic Dynamo', *J. Appl. Mech. Tech. Phys.* **14**, 775–779.

Simonyi, K.: 1990, *Kulturgeschichte der Physik*, Urania, Leipzig, Jena, Berlin, p. 343.

Steenbeck, M., Krause, F., and Rädler, K.-H.: 1966, 'A Calculation of the Mean Electromotive Force in an Electrically Conducting Fluid in Turbulent Motion, under the Influence of Coriolis Forces', *Z. Naturforsch.* **21a**, 369–376.

Steenbeck, M., Kirko, I. M., Gailitis, A., Klawina, A. P., Krause, F., Laumanis, I. I., and Lielausis, O. A.: 1967, 'An Experimental Verification of the α-Effect', *Monats. Dt. Ak. Wiss.* **9**, 716–719.

Steenbeck, M.: 1975, Letter to H. Klare, President of the Academy of Sciences of the GDR, p. 2, translation from the German original: "...daß der Aufwand für einen derartigen Versuch beträchtlich sein müsse - ein Kessel mit etwa 10 m^3 flüssigem Natrium und einer Umwälzpumpenleistung von nicht weniger als 10 m^3/sec."

Stefani, F., Gerbeth, G., and Gailitis, A.: 1999, 'Velocity Profile Optimization for the Riga Dynamo Experiment', in A. Alemany, Ph. Marty, and J. P. Thibault (eds.), *Transfer Phenomena in Magnetohydrodynamic and Electroconducting Flows*, Kluwer, Dordrecht, pp. 31–44.

Stieglitz, R. and Müller, U.: 2001, 'Experimental Demonstration of a Homogeneous Two-Scale Dynamo', *Phys. Fluids* **13**, 561–564.